Current **A**pplied **S**cience and **T**echnology e-ISSN: 2586-9396

Curr. Appl. Sci. Technol. ….., Vol... (No...), e0268928

Research article

Designing a Novel Schiff Base and Metal Complexes Derived from Drug Scaffold as Antioxidant Activity and Eco-Conscious Corrosion Inhibitors

Hawraa Mahdi Alabidia[1]* and Layla Ali Mohammedb[2]

[1]Department of Chemistry, Faculty of Science, University of Kufa, Iraq
[2]Department of Chemistry, College of Education for Girls, University of Kufa, Iraq

Received: 25 August 2025, Revised: 10 November 2025, Accepted: 25 November 2025, Published: 18 February 2026

Abstract

The article involves a novel synthesized Schiff base from a pharmaceutical compound, involving the condensation of amoxicillin with 4-(dimethylamino)-2-hydroxy aldehyde in a basic medium. Spectroscopic techniques such as elemental analysis, mass spectrometry, 1H-NMR, FT-IR, and UV-Vis spectrometry were used to characterize the new compound. These methods helped identify the formation of copper (II), silver (I), and gold (III) complexes with the Schiff base ligand (Amox-S). All compounds were evaluated for antioxidant activity using DPPH radical scavenging, showing 71%-86% activity, which was considered good and comparable to the standard ascorbic acid. The corrosion inhibition ability of the Schiff base and its Cu(II) complex on carbon C45 in acidic media (1M hydrochloric acid) was also examined using weight loss measurements at $1x10^{-4}$ - $1x10^{-3}$ M, for varying immersion times (1-10 days) at lab temperature of 25±2°C to determine the most effective concentration. It was found that the optimal concentration of the ligand and its complex as anti-corrosives was $1x10^{-3}$ M, which significantly enhanced the protective qualities of the coating. This optimal concentration was then evaluated for corrosion protection using polarization methods and the absence and presence of the Schiff base ligand and its copper(II) complex at three temperatures (293, 303, and 313 K). The Amox-S maintained an inhibition efficiency of 91-92% across the temperature range, whereas the Cu-complex exhibited slightly superior performance with IE% values of 93-94%.

Keywords: amoxicillin; Schiff base; spectrophotometric studies; complexes; antioxidant; anticorrosion

1. Introduction

Schiff bases, which are distinguished by the presence of the imine (-C=N-) functional group, are a significant class of compounds that have attracted a lot of interest in coordination and medicinal chemistry due to their wide range of biological activities, simplicity of synthesis, and structural versatility (Younus et al., 2023; Mushtaq et al., 2024). The presence of heteroatoms like nitrogen, oxygen, and sulfur in heterocyclic rings improves the chemical stability of drugs and offers more donor sites; consequently, Schiff

*Corresponding author: E-mail: aliphd256@gmail.com
https://doi.org/10.55003/cast.2026.268928

bases containing heterocyclic moieties often exhibit high biological efficiency, which contributes to enhanced therapeutic efficacy and greater selectivity in their pharmacological applications (Malik et al., 2018; Soroceanu & Bargan, 2022; Ali et al., 2023). Their bio-reactivity is further enhanced through the formation of strong hydrogen bonding interactions. Moreover, these compounds are capable of stabilizing complex molecular architectures via efficient π–π stacking interactions, thereby contributing to their overall structural integrity and biological efficacy (Ramadan et al., 2025). Amoxicillin, a widely used β-lactam derivative, serves as a valuable scaffold for structural modification owing to its free primary amine group and proven clinical efficacy (Karaman et al., 2015).

Amoxicillin's derivatization from Schiff base synthesis introduces more heterocyclic functionality that could improve its biological characteristics. These changes might deal with the limitations associated with standard β-lactam antibiotics, such as their limited anticancer effect and bacterial resistance (Podolski-Renić et al., 2024; Presenjit et al., 2024). In addition to the fact that the formation of coordination complexes with Schiff bases derived from amoxicillin enhanced their biological potential and demonstrated antioxidant and anticancer properties. Therefore, Schiff base complexes are particularly interesting (Savcı et al., 2022; Moreno-Narváez et al., 2025).

Schiff bases, which are practically derived from pharmaceuticals, have also been used as effective and environmentally friendly corrosion inhibitors (Betti et al., 2023; Abd El-Zahir et al., 2024). There is significant interest in replacing harmful inhibitors with non-toxic alternatives. Therefore, the use of many drugs as corrosion inhibitors, such as amoxicillin and its derivatives, has gained great importance (Abdallah et al., 2023; Alamry et al., 2023). By condensing amoxicillin with an aromatic aldehyde, a new heterocyclic Schiff base was synthesized in this study. This was followed by complexation with Cu(II), Ag(I), and Au(III) ions. A variety of spectroscopic and analytical techniques were used to characterize the resulting compounds. These were evaluated for their antioxidant properties using DPPH radical scavenging tests. Additionally, the Schiff base and Cu(II)-complex were assessed as anticorrosion agents in HCl solutions on mild steel through a weight loss technique. The results highlight the heterocyclic Schiff base and its complexes as promising candidates for developing anticancer and antioxidant medications. Establishing the relationship between complex formation and the biological/corrosion inhibition properties can expand their potential as multifunctional agents with both protective and biomedical applications.

2. Materials and Methods

In this search, all starting materials were obtained from significant companies such as Fluka, BDH and Sigma Aldrich, and mild steel plates (C45) were used for the weight loss method. All chemicals used were used without further purification.

2.1 Chemical synthesis

2.1.1 Synthesis of a new Schiff base ligand

Amox-Schiff base ligand was synthesized according to Chaudhary and Mishra (2017) by dissolving the amoxicillin trihydrate (1 mmol) in 20 mL of absolute methanol and stirring it under hot conditions for 3 h. The pH was adjusted to neutral by adding 0.1N NaOH solution. 4-(dimethylamino)salicylaldehyde (1 mmol) was added slowly to the well dissolved amoxicillin trihydrate solution and refluxed for 15 h at 55^{o}C. A light purplish red solution

was left undisturbed for crystallization, then collected and recrystallized using methanol and later by acetone solvent.

Yield: 70%, light red powder, m.p:141-143, $C_{25}H_{28}N_4O_6S$ (512.58 g/mol), Cald.C(58.58%), H(5.51%), N(10.94), O(18.73%), S(6.26%); Found: C(58.91%), H(5.89%), N(11.23%), O(18.93%), S(6.59%), FT-IR (KBr) (cm^{-1}): 3330 (O-H and N-H), 2931 and 2882 (C-H aliph), 1735 (C=O β-lactam ring), 1622 (CH=N). ^{1}H-NMR (400 MHz, d^6 DMSO): 8.10 (OH-arom), 6.08-7.45 (H-arom), 9.64 (CH=N), 13.41 (COOH), 8.19 (N-H amide), 4.24 (CO-CH), 4.21 (N-CH), 3.52 (CH-C=O), 1.14 (2CH3), 3.39 (CH-S).

2.1.2 Synthesis of metal complexes

The metal complexes were prepared by slowly adding 1 mmol of Cu(II), Ag(I), and Au(III) metal salts in 15 mL of methanol to 1 mmol of Schiff base (Amox-SL) in 30 mL of warm methanol with stirring. Sodium hydroxide (0.1% in methanol) was used to adjust the solution pH to 7, followed by refluxing at 45°C for 4-6 h. The resulting complexes were collected, washed, purified (Reiss et al., 2015), and dried overnight at 50ºC, as shown in Figure 1.

Cu(II) complex: Yield 65%, greenish earthy powder, m.p:141-143, $C_{25}H_{29}N_4O_7SCuCl$ (627.59), Cald.C(47.77%), H(4.65%), N(8.91), O(17.82%), S(5.10%), Cu(10.11%), Cl(5.64%) ; Found: C(47.94%), H(4.88%), N(9.23), O(18.092%), S(5.34%), Cu(10.42%), Cl(5.91%), FT-IR (KBr) (cm-1): 3238 (OH), 2926 and 2852 (C-H, aliph), 1610 (HC=N), 1521 (C=C, arom), 563(M-O), 495(M-N).

Ag(I) complex: Yield 68%, greenish brown powder, m.p:141-143, $C_{25}H_{27}N_4O_6SAg$ (619.44), Cald.C(48.48%), H(4.39%), N(9.05%), O(15.50%), S(5.18%), Ag(17.41%); Found: C(49.01%), H(4.91%), N(9.43%), O(15.96%), S(5.47%), Ag(17.62%), FT-IR (KBr) (cm-1): 3414 (OH), 2926 and 2852 (C-H, aliph), 1566 (C=N), 1516 (C=C, arom), 530(M-O), 432(M-N).

Au(III) complex: Yield 67%, brown powder, m.p:141-143, $C_{25}H_{27}N_4O_6SAuCl_2$ (779.44), Cald.C (38.53%), H(3.49%), N(7.19%), O(12.32%), S(4.12%), Au(25.27%), Cl(9.10%) ; Found C(39.12%), H(3.87%), N(7.69%), O(13.01%), S(4.54%), Au(25.64%), Cl(9.89%), FT-IR (KBr)(cm-1): 3412 (OH), 2926 and 2852 (C-H, aliph), 1598(C=N), 1510 (C=C, arom), 540(M-O), 435(M-N).

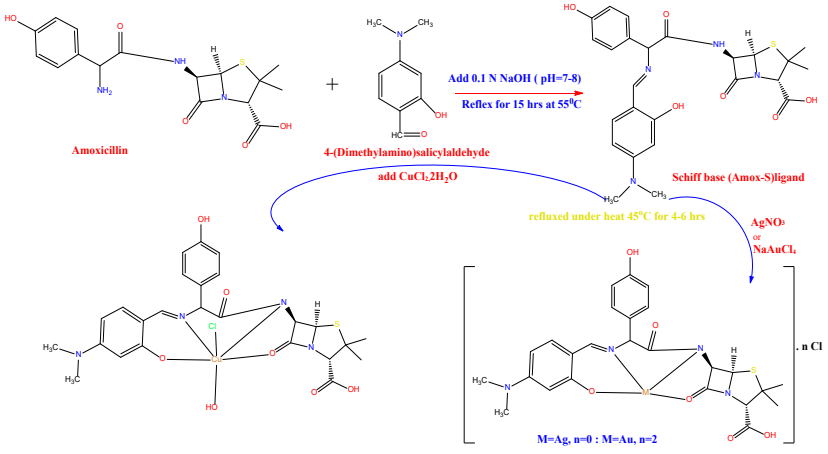

Figure 1. Synthesis for the Schiff base and its metal complexes

2.2 Evaluation of antioxidant activity

The antioxidant activity of the Schiff base and their complexes was evaluated using 1,1-diphenyl-2-picrylhydrazyl (DPPH) assay which was prepared in methanol at concentrations ranging from 50 to 200 µg/mL (Hilal & Kareem, 2025). An amount of 2 mL of synthesized compounds was mixed with 1 mL of DPPH solution at a concentration of 0.003% w/v. Ascorbic acid was used as the reference antioxidant, and the mixtures were incubated at room temperature in the dark before the absorbance at 517 nm was measured to assess the extent of radical scavenging. The percentage of inhibition (I%) was calculated using equation (1), where Ac is the absorbance of the control and As is the absorbance of the sample:

$$\mathrm{I\%} = \frac{\mathrm{Ac-As}}{\mathrm{Ac}} \mathrm{x}\ 100 \quad (1)$$

All experiments were carried out in triplicate (n = 3), and the results were expressed as mean±standard deviation (SD). The obtained data were statistically processed and plotted using Microsoft Excel 2019. Statistical comparisons were evaluated by one-way analysis of variance (ANOVA).

2.3 Corrosion measurement

2.3.1 Weight loss method

Corrosion tests were performed using C45 carbon steel alloy; the chemical composition (wt %) of the alloy is shown in Table 1.

Table 1. Chemical composition of carbon steel C45

Metal	C%	Si%	Mn%	S%	Cu%	Ni%	Cr%	Fe%	P%
Carbon Steel 45	0.36-0.42	0.15-0.30	1.00-1.40	0.05	0.50	0.20	0.20	96.88-97.49	0.05

In this method, the initial weight of thoroughly polished carbon steel samples (2 cm x 2 cm x 0.1cm) was measured before immersing them in corrosive acid solutions prepared from 1 M hydrochloric acid, with and without certain inhibitor concentrations ($1x10^{-4}$ -$1x10^{-3}$ M), with varying immersion times (1-10 days) at lab temperature (25±2°C). The corrosion rate (CR), the percentage inhibition efficiency (IE%) were calculated using equations (2,3) (Affat, 2022):

$$\mathrm{CR\ (mm/year)} = \frac{87.6 \times \Delta \mathrm{W}}{\rho \times \mathrm{A} \times \mathrm{t}} \quad (2)$$

Where ΔW is the weight loss (g) before and after immersion in the test solutions ΔW= Winitial − Wfinal, CR is the corrosion rate, A is the area of the specimen (cm^2), ρ is the density of the alloy in g/cm^3 and t is the immersion time (days). The inhibition efficiency (IE%) was computed using equation (3) (Alfakeer et al.,2020):

$$\mathrm{IE\%} = \frac{\mathrm{CRblank} - \mathrm{CRinh.}}{\mathrm{CRblank}} x100 \quad (3)$$

$$\theta = \frac{\mathrm{CRblank} - \mathrm{CRinh}}{\mathrm{CRblank}} \quad (4)$$

CRblank is the corrosion rate in the absence of inhibitor and CRinh is the corrosion rate in the presence of inhibitor and θ is the surface coverage. Each test specimen was taken out every 24 h, washed with distiled water and rinsed with acetone, dried and re-weighed (equation 4).

2.3.2 Polarizatıon curves

The corrosion current density (icorr) and corrosion potential (Ecorr) were determined by extrapolating the cathodic and anodic Tafel plots in both the absence and presence of inhibitor molecules in HCl (1M) solution. The anodic (ba) and cathodic (bc) Tafel slopes were also calculated from Figures 11-13 and Table 8 shows the data for corrosion potential Ecorr (mV), corrosion current density icorr (A/cm²), cathodic and anodic Tafel slopes (mV/Dec), and protection efficiency PE% (Khudhair & Al-Sammarraie 2019; Khudhair et al., 2020):

$$\%\mathrm{IE} = \frac{(\mathrm{icorr})\mathrm{o} - (\mathrm{icorr})}{(\mathrm{icorr})\mathrm{o}} * 100 \quad (5)$$

Where (icorr)o is the corrosion current density in the absence of inhibitors, (icorr) is the corrosion current density in the presence of inhibitors and %IE is inhibition efficiency. The tested sample was inserted into corrosion cell in which the diameter of the exposed surface to the solution was 16.55cm^2 (equation 5).

3. Results and Discussion

3.1 Chemistry of synthesized compounds

This work describes the synthesis of a new Schiff base derived from amoxicillin and 4-(dimethylamino)salicylaldehyde in a 1:1 molar ratio, yielding the new organic compound in good yield. It was observed that the yield of the ligand was 70% and the yields of the prepared complexes were less than 65-68% (Table 2). This could be due to the multiple steps of preparation, the possibility of side reactions occurring during the coordination with the metal ion, and the loss of part of the complex during the filtration, washing, or recrystallization processes. It also reports three complexes of the new Schiff base with Cu(II), Ag(I), and Au(III) metal ions, which serve as effective antioxidants and anticorrosion agents.

3.2 NMR spectra

The ^{1}H-NMR spectra of Schiff base observed were singles in the range of 6.08-7.45 ppm due to the aromatic hydrogen atoms and single peak attributed to hydroxyl group appeared

Table 2. The physical properties of new Schiff base (Amox-SL) and its complexes

Compound	Chemical Formula	M.wt	Color	m.p °C	Yield %
Amox-SL	$C_{25}H_{28}N_4O_6S$	512.17	Purple red	144-146	70
[Cu(AmoxS)Cl(H_2O)]	$C_{25}H_{29}N_4O_7SCuCl$	627.07	Greenish earthy	>250	65
[Ag(Amox-S)]	$C_{25}H_{27}N_4O_6SAg$	619.44	Greenish brown	>250	68
[Au(Amox-S)]Cl_2	$C_{25}H_{27}N_4O_6SAuCl_2$	779.44	Brown	>250	67

at 8.10 ppm. The proton of azomethine (CH=N) showed up as a single at 9.64 ppm, single peak attributed to hydroxyl group of carboxylic appeared at 13.41 pm (Alabidi et al., 2023). The N-H amide group appeared at 8.19 ppm, and other signals appeared at 4.24, 4.21 and 3.52 ppm were due to protons (CO-CH and N-CH) on the β-lactam ring and CH-C=O, respectively, while the singlet signals of methyl groups appeared at 1.09 and 1.14 ppm ($2CH_3$), as shown in Figure 2. It is worth noting that the proton of Ar-OH resonates at 7.45 ppm. The peaks appeared at 3.39 ppm can be attributed to (CH-S) group (Chavelas-Hernández et al., 2020; Kalluru et al., 2023).

3.3 FT-IR spectra

FT-IR spectra of the complexes were compared with the spectrum of the free ligand to identify any changes that may have occurred during the complexation process. The spectra displayed significant and distinctive features in the chemical structure of Amox-SL and its complexes, confirming the formation of the complexes. A broad, intense band in the region corresponds to O-H and N-H stretching at 3200-3400 cm^{-1}, and the specific bands were observed at 1622 cm^{-1} corresponds to ν(CH=N), and 1735 cm^{-1} corresponds to ν(C=O β-lactam ring). These bands showed shifts in the IR spectra of the synthesized complexes, with ν(C=N) shifting to a lower wave number and ν(C=O β-lactam ring) also shifting to a lower value in all the complexes, indicating coordination (Reiss et al., 2014). New absorption bands ν(M-O) and ν(M-O) appeared at 530-563 cm^{-1} and 432-495 cm^{-1}, respectively, in the spectra of the complexes, indicating ligand coordination through nitrogen and oxygen (Alabidi et al., 2018). The results are shown in Table 3.

3.4 Mass spectra

Figure 3, Figure 4 and Table 4 show the mass spectrum of Amox-S ligand and Ag(I) complex recorded at room temperature, and Figures 5 and 6 present the proposed mass fractionation pathway. The peaks obtained confirm the formula which were proposed for the prepared compound. The molecular ion peak at m/z 512.4 confirms the reposed formula of the ligand, yet its low relative abundance is consistent with observations that high molecular weight compounds, especially those subjected to intense ionization energy and containing multiple heteroatoms, tend to produce weaker molecular ion signals (Patriarca & Hawkes, 2020).

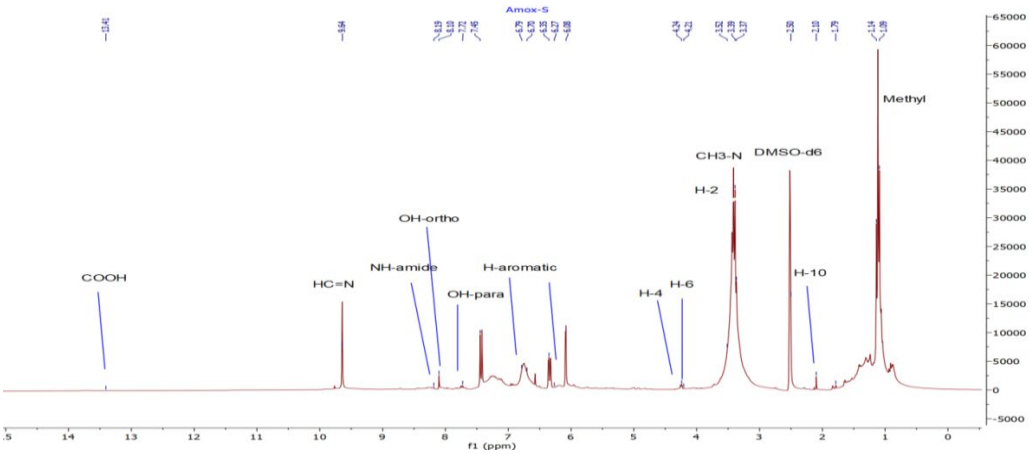

Figure 2. ^{1}H-NMR spectra of Amox-S ligand

Table 3. Observed IR frequencies for Amox-S ligand and its metal complexes in cm^{-1}

Compound	ν(O-H) ν(N-H)	ν(C=C)	ν(C=N)	ν(C=O)β-lactam est.	ν(M-O)	ν(M-N)
Amox-S(L)	3302	1517	1622	1735	-	-
[CuLCl(H_2O)]	3238	1521	1610	1720	563	495
[AgL]	3414	1516	1566	1629	530	432
[AuL]Cl_2	3412	1510	1598	1630	540	435

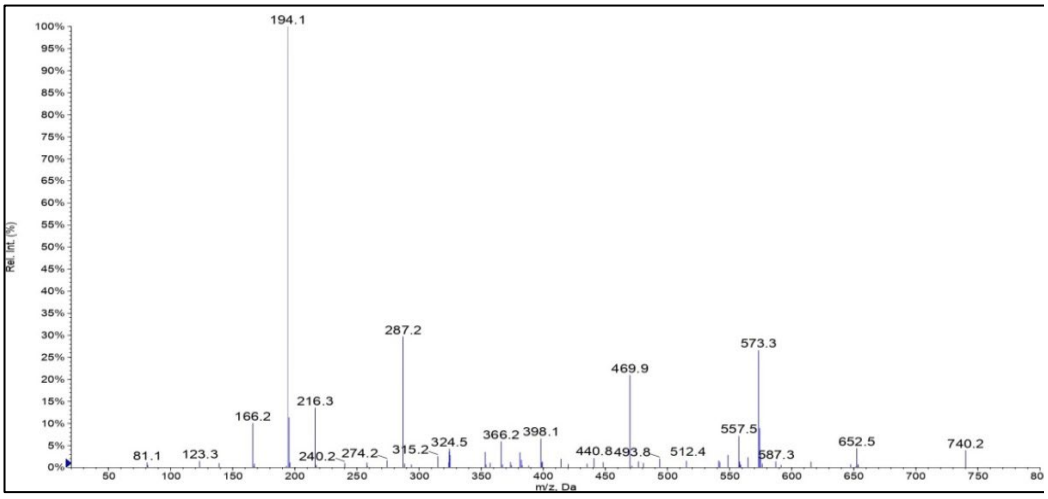

Figure 3. Mass spectra of Amox-S ligand

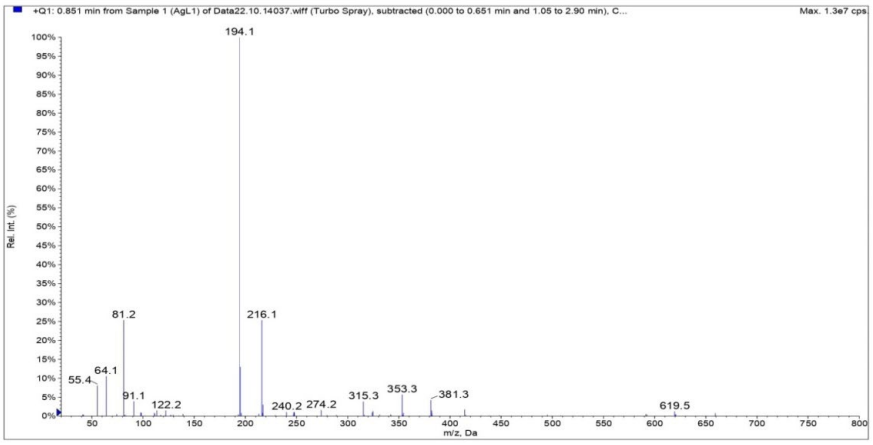

Figure 4. Mass spectra of Ag(I)-complex

Table 4. The mass spectral data of Amox-S and Ag(I)-complex

Amox-S			Ag(I)-Complex		
Proposed Fragment	**m/z**	**Relative Abundance**	**Proposed Fragment**	**m/z**	**Relative Abundance**
$C_{25}H_{28}N_4O_6S$	512.58	2%	$C_{25}H_{27}AgN_4O_6S$	619.07	1.40%
$C_{25}H_{25}N_4O_5S^+$	493.56	1.40%	$C_{20}H_{19}N_3O_3S$	381.11	5.50%
$C_{23}H_{25}N_4O_5S^+$	469.54	20.70%	$C_{20}H_{23}N_3OS$	353.16	7.10%
$C_{21}H_{20}N_4O_5S^{+2}$	440.11	1.40%	$C_{13}H_{19}N_2O_5S^+$	315.1	2%
$C_{20}H_{22}N_4O_3S$	398.48	6.90%	$C_{13}H_{10}N_2O_3S^+$	274.04	1.40%
$S_5O_3N_{20}H_{16}C^{\bullet}$	366.11	6.90%	$C_{11}H_{16}N_2O_2S$	240.09	1.40%
$S_3O_4N_{20}H_{14}C^{\bullet}$	324.13	4.80%	$C_7H_8N_2O_4S$	216.02	24.10%
$S_5O_2N_{16}H_{14}C^{\bullet}$	324.35	4.80%	$C_{14}H_{12}N^+$	194.1	100%
$C_{13}H_{19}N_2O_5S^+$	315.1	2%	$C_8H_{12}N^+$	122.1	1.40%
$C_{11}H_{17}N_3O_4S$	287.05	31.03%	$C_7H_7^+$	91.05	3.50%
$C_{10}H_{16}N_3O_4S^+$	274.09	1.40%	$C_6H_9^+$	81.07	26.20%
$C_{11}H_{16}N_2O_2S$	240.09	0.70%	$C_5H_4^{+\bullet}$	64.03	10.30%
$C_7H_8N_2O_4S$	216.02	13.80%	$C_4H_7^+$	55.05	9%
$C_8H_{12}N_2O_3S$	216.02	13.80%			
$C_{14}H_{12}N^+$	194.1	%100			
$C_7H_6N_2OS^{2+}$	166.2	10.30%			
$C_9H_{11}NO_2$	166.08	10.30%			
$C_8H_{13}N$	123.2	1.40%			
$C_5H_2NOS^{2+}$	123.98	1.40%			
$C_6H_9^+$	81.14	0.70%			

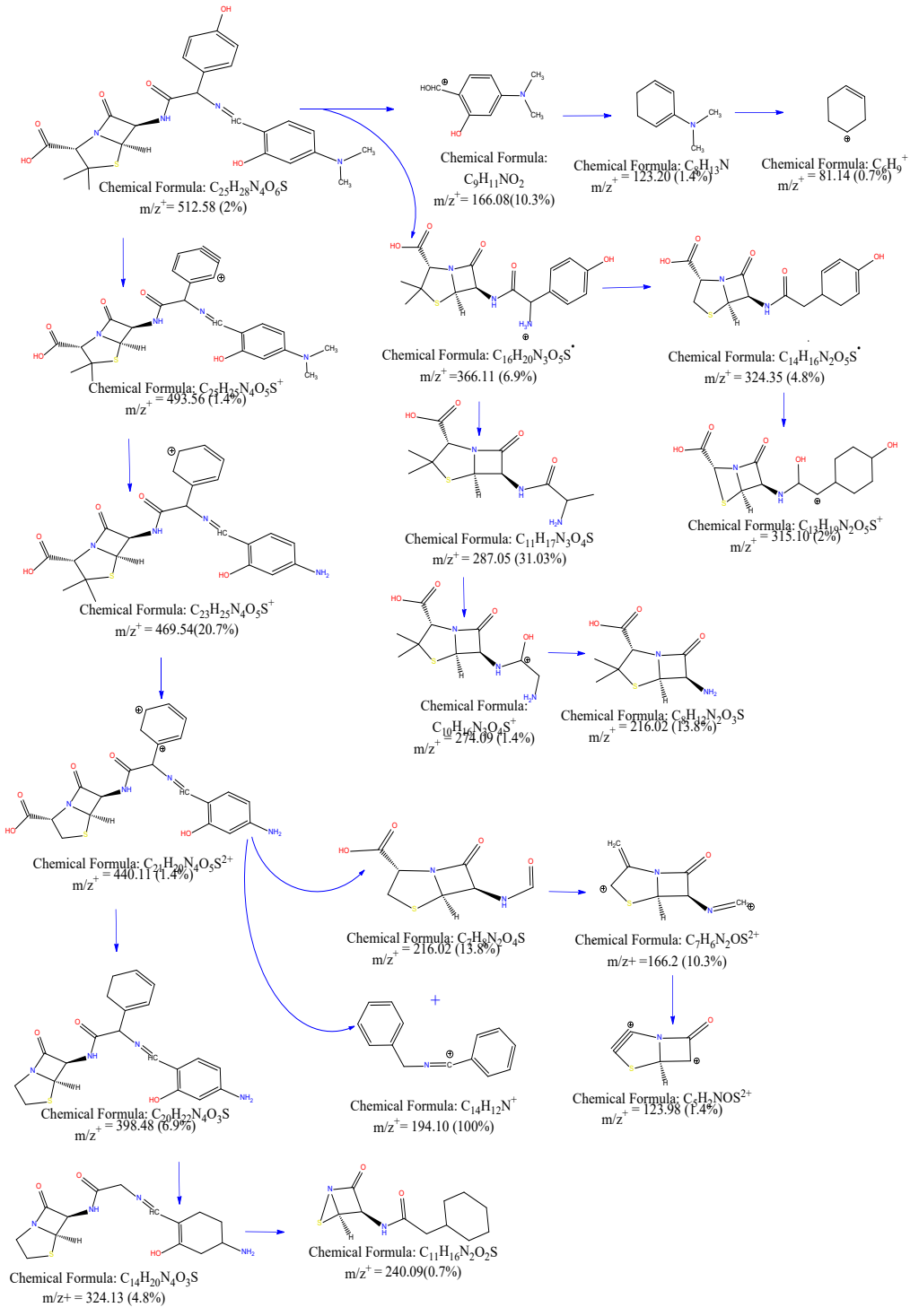

Figure 5. Mass spectrum fragmentation of Amox-S ligand

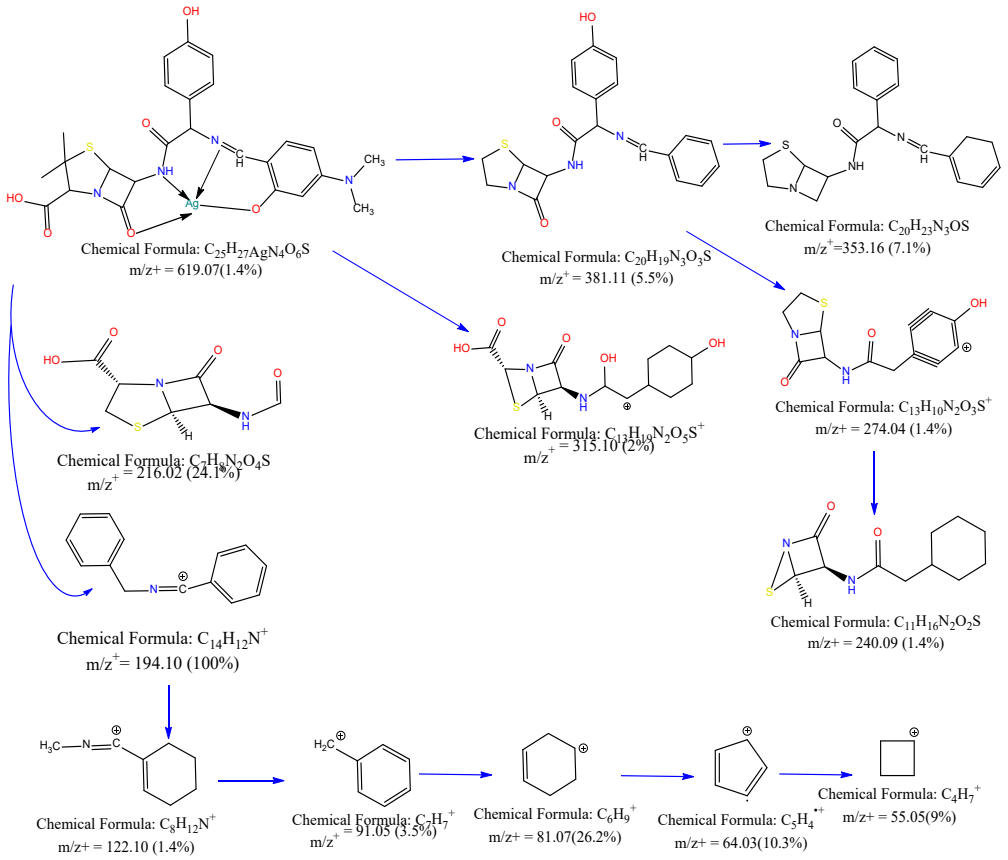

Figure 6. Mass spectrum fragmentation of Ag(I)-complex

3.5 Absorption spectra of Amox-SL and its complexes

The electronic absorption of Amox-S clearly shows two bands, as shown in Figure 7 at different wavelengths. The π-π* transition was assigned to the first band, which appeared at 403 nm, while the other band observed at 539 nm, assigned n- π* transition, which represents the λ_{max} of ligand (Kyhoiesh & Al-Adilee 2021). The π-π* transition displayed a red shift as a result of chelation when binding with metal ions (Table 5). The copper(II) complex spectrum shows one broad peak at 624 nm, attributed to the $^2E_2g \rightarrow {}^2T_2g$ transmissions in a distorted octahedral stereochemistry around ion of the Cu(II). A band at 458 nm is attributed to charge-transfer, fundamentally of the L→Cu kind (Figure 7) (Hernández et al., 2024). The Ag(I) complex spectrum displays a strong intense charge transfer transmissions (LMCT) bands at 587 nm. The Au(III) complex exhibited one band at 585 nm, which was assigned to the $^1A_1g \rightarrow {}^1B_1g$ transition (Hadi et al., 2021). This complex has a diamagnetic momentum and is square planer. The metal complexes were air stable at room temperature and were insoluble in water but soluble in ethanol, methanol and DMSO. The molar conductivities of 10^{-3} mol/mL solutions of Cu(II) and Ag(I) complexes in ethanol showed nonelectrolyte nature (Kanagavalli et al., 2024) and Au(III) complex showed ionic properties (1:2) (Kzar et al., 2023), which confirmed the validity of the proposed structures, as shown in Table 5.

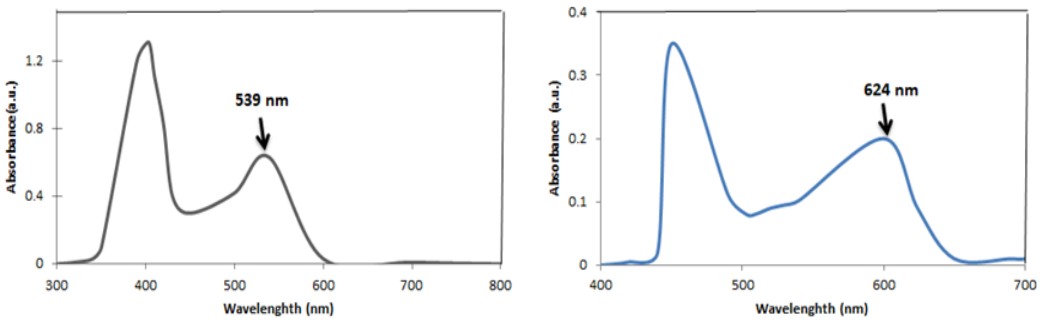

Figure 7. Electronic spectra of Amox-S ligand and its Cu(II)-complex

Table 5. The electronic, magnetic moment, and conductivity data of the prepared compounds ethanol solvent

Compound	λ nm	ν cm^{-1}	Transition	Stereochemistry	μ_{eff}	Λm S.cm^2.mol^{-1}
Amox-S(L)	539	18552.875	n- π*	-	-	-
[CuLCl(H_2O)]	624	16025.641	$^2E_2g \rightarrow {}^2T_2g$	Octahedral	1.83	9.44
[AgL]	587	17035.775	LMCT	Tetrahedral	Dia	8.57
[AuL]Cl_2	585	17094.017	$^1A_1g \rightarrow {}^1B_1g$	Square planer	Dia	80.7

3.6 Evaluation of the antioxidant activity of Amox-S ligand and its metal complexes compared to ascorbic acid

DPPH radical test affords an easy and rapid means to evaluate antioxidants because DPPH is a stable purple colored free radical that is usually employed in chemical analysis for the detection of radical scavenging activity. DPPH is converted into a colorless form after its reaction with antioxidants. The reduction capability of DPPH radicals is evaluated from the decrease in its absorbance at 517 nm, which is induced by antioxidants. The antioxidant assay study was carried out using different concentrations of the ligand and its complexes with DPPH radicals and compared with ascorbic acid as the standard. Table 6 and Figure 8 present the inhibition efficiency values (I%) of the Amox-S ligand and its metal complexes (Cu(II), Ag(I), and Au(III)-complexes), which were evaluated as potential antioxidants through their free radical scavenging activities, and compared to the standard ascorbic acid. The assessment was conducted at four concentrations: 50, 100, 150, and 200 ppm. For every concentration, the mean values obtained show the average percentage of DPPH radical scavenging activity, while the standard deviation (SD) shows how repeatable the measurements really are. The accuracy and dependability of the experimental results were confirmed by the comparatively low SD values (<10%). The findings revealed notable differences in the antioxidant efficiency across compounds and concentrations (Al-Daffay et al., 2025). At 50 ppm, the Au(III)-complex exhibited the highest inhibition efficiency (86.08%), outperforming all other tested compounds, including

ascorbic acid (65%). This suggests that Au(III), due to its high oxidation potential, can rapidly neutralize free radicals even at low concentrations (Kyhoiesh & Al-Adilee 2023). The Cu-complex (78.95%) and Ag-complex (73.95%) also showed good activity, with the Amox-S ligand recording 72.03%. These results indicate that metal coordination enhances antioxidant behavior at low concentrations. At 100 ppm, the Au(III)-complex remained the most effective (84.63%), closely followed by the Amox-S ligand (83.05%). This reinforces the synergistic effect of the functional groups (–NH and –OH) present in the ligand, contributing significantly to radical scavenging (Kasare et al., 2019). At 150 ppm, the Cu- and Ag-complexes demonstrated moderate activity, while ascorbic acid showed limited improvement (85.30%), Amox-S ligand (84.36%) and Cu-complex (83.44%) maintained consistent and high antioxidant efficiency, suggesting structural stability (Todorov et al., 2023). At 200 ppm, ascorbic acid demonstrated a near-complete scavenging effect (98.20%), asserting its position as the most potent antioxidant at higher concentrations. However, both the Amox-S ligand (87.41%) and the Cu-complex (85.09%) retained strong inhibitory activity, making them viable alternatives (Tabrizi et al., 2019; El-Lateef et al., 2023).

Table 6. The percentage of scavenging activity of Amox-S ligand and its complexes

Conc. (ppm)	Amox-SL I%	Cu-complex I%	Ag-complex I%	Au(III)-complex I%	Ascorbic acid	Mean	SD
50	72.03	78.95	73.95	86.08	65	75.202	7.875
100	83.05	79.5	74.8	84.63	73	78.996	5.049
150	84.36	83.44	79.16	71.24	85.30	80.7	5.786
200	87.41	85.09	71.50	84.03	98.20	85.246	9.525

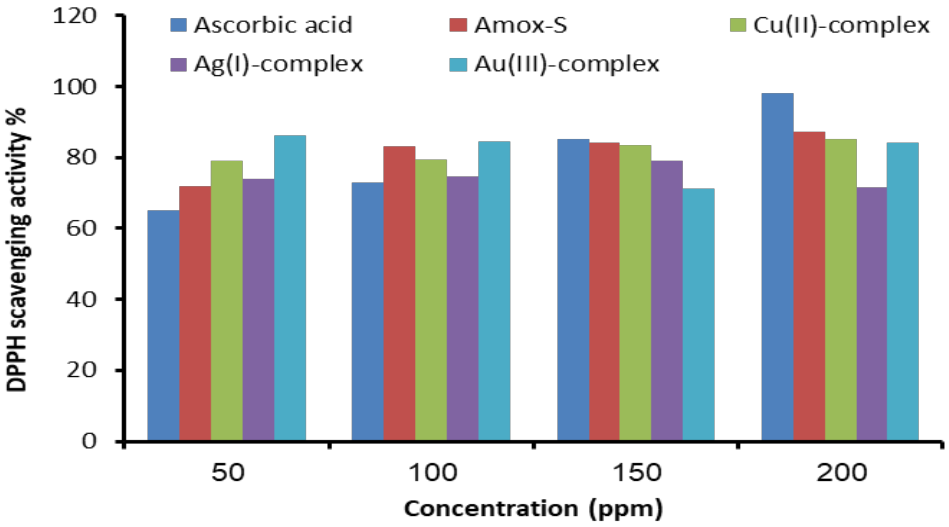

Figure 8. Scavenging activity of the Amox-S ligand and its Cu(II), Ag(I) and Au(III) complexes compared with ascorbic acid

3.7 Corrosion inhibitor

3.7.1 Weight loss measurements

The corrosion resistance of carbon steel (ST45) in 1M hydrochloric acid solution was evaluated experimentally in both the presence and absence of two synthetic compounds (Amox-ligand and Cu-complex) at different concentrations. The weight loss method for assessing metal corrosion in corrosive environments was used to investigate these compounds' capability as corrosion inhibitors. As the inhibitor concentration increased, the inhibition efficiency of both Amox-S and its Cu(II) complex improved, exceeding 83.87% in 1 M HCl even at low concentrations. The optimum efficiency was observed at 1×10^{-3} M (Figure 9). The results indicate that the corrosion rate decreases with increasing inhibitor concentration due to the saturation of active sites on the steel surface, where adsorbed inhibitor molecules form a protective layer that limits metal–acid interaction (Al-Amiery et al., 2022; Youssif et al., 2023). The inhibition mechanism of the inhibitors can be interpreted through these molecules containing heteroatoms such as oxygen, nitrogen, and sulfur (O, N, S), which have non-bonding electron pairs. These lone pairs are capable of interacting with the vacant d-orbitals of the metal atoms on the surface (Farhan et al. 2024). These interactions enhance the bonding of organic inhibitor molecules to the metal surface, resulting in a protective layer that effectively isolates the metal from corrosive substances in the environment, thereby reducing the rate of corrosion (Ahmed et al. 2024; Shwetha et al., 2024).

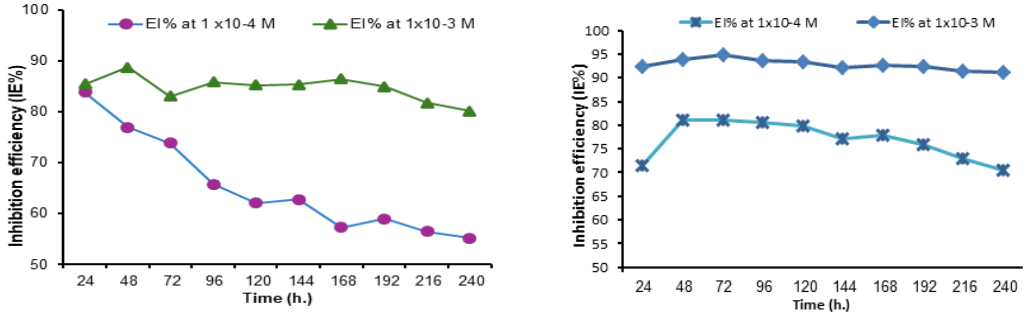

Figure 9. Inhibition efficiency (IE%) as a function of immersion time (24-240 h) at concentrations of 1×10^{-4} M and 1×10^{-3} M for (A) the Amox-S ligand and (B) Cu(II)-complex

Basic information on the interaction between the inhibitors and carbon mild steel surface can be provided by the adsorption isotherm (Figure 10). The degree of surface coverage (θ) at different concentrations was calculated from weight loss method (equation 4). The adsorption equilibrium constant value was obtained through a straight line of C/θ and C as expressed in equation 6.

$$\frac{C}{\theta} = \frac{1}{\text{Kads}} + C \qquad (6)$$

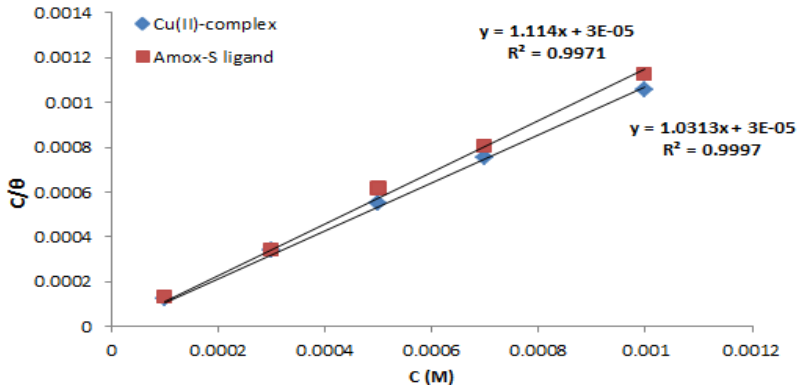

Figure 10. Langmuir adsorption isotherm on the C45 steel surface of Amox-S ligand and its Cu-complex

Where C is the inhibitor concentration in molar, θ the surface coverage and Kads is the equilibrium constant of the adsorption process. Kads is related to the standard Gibbs free energy of adsorption (ΔG_{ads}) by equation 7 (Farhan et al., 2024):

$$\Delta G_{ads} = -RT \ln (55.5\ K_{ads}) \quad (7)$$

The negative ΔGads values shown in Table 7 are consistent with the spontaneity of the adsorption process and the stability of the adsorbed layer on the C45 surface.

Table 7. Thermodynamic parameters using Langmuir adsorption isotherm on the C45 steel surface in 1M HCl at different concentrations of Amox-S ligand and its Cu-complex

Inhibitor	Temp.(K)	K_{ads}	ΔG_{ads}
Amox-S ligand	298	33333.33	-35.753
Cu-complex	298	33333.33	-35.753

3.7.2 Potentiodynamic polarization measurements

The polarization data, including the corrosion potential (Ecorr), corrosion current densities (icorr), anodic (bc), cathodic (ac) Tafel slopes, corrosion Rate (CR) and Resistance for C45 carbon steel alloy in 1 M HCl solution in the absence and presence of $1X10^{-3}$ M of Amox-S ligand and Cu-complex inhibitors are given in Table 8 and Figures 11-13 as polarization curves.

The corrosion behavior of C45 mild steel in 1 M HCl was examined using potentiodynamic polarization at 293-313 K, both without and with the Schiff base ligand Amox-S and its Cu(II) complex. The inhibitors markedly reduced corrosion rates, as reflected in the electrochemical parameters. The corrosion potential (−Ecorr) shifted from −0.427 to −0.385 V for the uninhibited steel to more negative values (−0.764 to −0.783 V) in the presence of Amox-S, suggesting a mixed-type inhibition mechanism with a predominant cathodic effect (El-Lateef et al., 2022; El Aloua et al., 2024). Similarly, the Cu(II) complex showed −Ecorr values between −0.657 and −0.645 V, confirming its strong adsorption and effective inhibition of the electrochemical corrosion reactions (Almomani et

Table 8. C45 carbon steel alloy in 1 M HCl solution in the absence and presence of $1x10^{-3}$ M of Amox-S ligand and Cu-complex as inhibitors at three temperatures (293, 303, and 313 K)

Comp.	Blank (Absence Inhibitors)			Amox-S			Cu-complex		
Temp.	293	303	313	293	303	313	293	303	313
-Ecorr((mV)	-0.427	-0.385	-0.425	-0.764	-0.765	-0.783	-0.657	-0.639	-0.645
Icorr((μA/cm^2)	493.9	563.2	620.6	39.43	45.76	54.91	30.32	38.30	49.53
Icorr./r(A/cm^2)	9.878E-4	0.001	0.001	7.885E-5	8.352E-5	1.098E-4	6.064E-5	7.660E-5	9.906E-5
Resis.(Ω)	70.31	28.96	57.49	1889	2195	2058	1843	1575	1592
-Bc((mV/Dec)	0.156	0.055	0.166	0.320	0.371	0.508	0.248	0.252	0.331
Ba((mV/Dec)	0.164	0.120	0.163	0.369	0.490	0.534	0.267	0.310	0.402
Corr.Rate(mm/y)	4.848	5.529	6.091	0.387	0.410	0.539	0.298	0.376	0.486
IE%	-	-		**92**	**92**	**91**	**94**	**93**	**92**

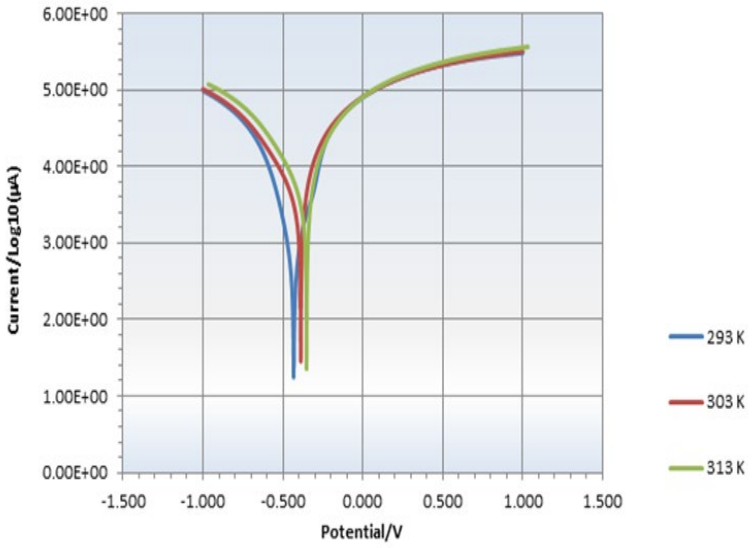

Figure 11. Polarization curves of C45 carbon steel alloy in the blank solution 1M HCl at temperatures of 293, 303, and 313 K

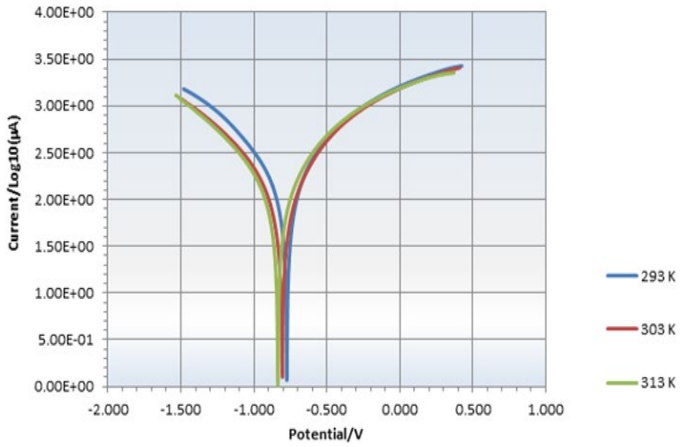

Figure 12. Polarization curves of C45 carbon steel alloy in the presence of 500 ppm of Amox-S inhibitor at temperatures of 293, 303 and 313 K

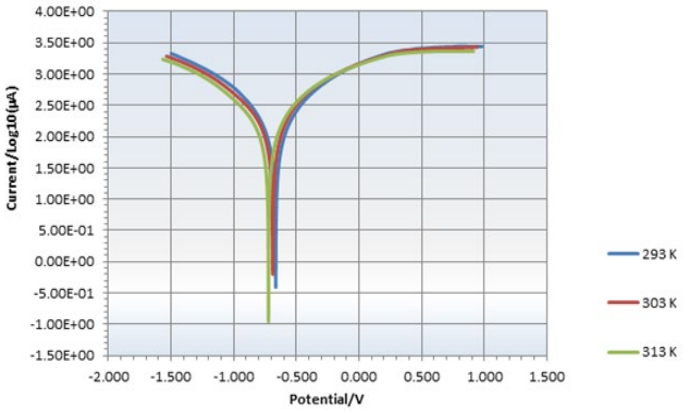

Figure 13. Polarization curves of C45 carbon steel alloy in the presence of 500 ppm of the Cu-complex inhibitor at temperatures of 293, 303, and 313 K

al., 2021). The corrosion current density (icorr) of the uninhibited system increased with temperature (493.9 to 620.6 μA/cm²), whereas a notable reduction was observed upon the addition of the inhibitors, indicating their pronounced protective efficiency (Go et al., 2020; Mahmoud et al., 2022). The inhibition efficiency (IE%) further supports these findings. Amox-S maintained an inhibition efficiency of 91-92% across the temperature range, whereas the Cu-complex exhibited slightly superior performance with IE% values of 93-94%. The improved efficiency of Cu-complex can be attributed to the increased adsorption strength and surface coverage resulting from the presence of the metal ion, which facilitates better interaction between the inhibitor and the steel surface through π-back bonding and d-orbital participation, in line with Pearson's Hard-Soft Acid-Base (HSAB) principle (Radi et al., 2022). This small decrease in efficiency with temperature increase might be due to partial desorption of the inhibitors at higher thermal energy, though the efficiency remains high overall, confirming the thermal stability of the inhibitor films (Verma et al., 2024).

3.7.3 Kinetic and thermodynamic analysis of the corrosion ınhibition process

To gain insight into the mechanism and energy dynamics of corrosion inhibition of C45 mild steel in 1 M HCl, kinetic and thermodynamic parameters were derived from the temperature-dependent corrosion rate data using Arrhenius and transition state models. These parameters help clarify whether the inhibition process involves physical or chemical adsorption and reveal how temperature influences inhibitor efficiency. The activation energy (Ea) of the corrosion process was determined using an Arrhenius equation 8 (Diki et al., 2021).

$$\ln icorr = \frac{-Ea}{R}.\frac{1}{T} + \ln A \tag{8}$$

A plot of ln(icorr) vs 1/T provides straight lines for calculating values of Ea, as shown in Figure 14. The blank solution (without inhibitor) exhibited a relatively low Ea of 8.717 kJ/mol), indicating a spontaneous and rapid corrosion process. In contrast, the presence of the Schiff base ligand Amox-S and its copper(II) complex significantly increased the activation energy to 12.6 kJ/mol and 18.69 kJ/mol, respectively. This suggests that both inhibitors raised the energy barrier for corrosion, thereby slowing the reaction. The higher Ea values point to the formation of a protective inhibitor layer that limits the accessibility of corrosive species to the steel surface. Moreover, the higher Ea for Cu-complex implies stronger interaction with the steel surface, likely due to enhanced π-backbonding and chelation effects from the Cu(II) ion (Emrayed et al., 2025; Lasri et al., 2025).

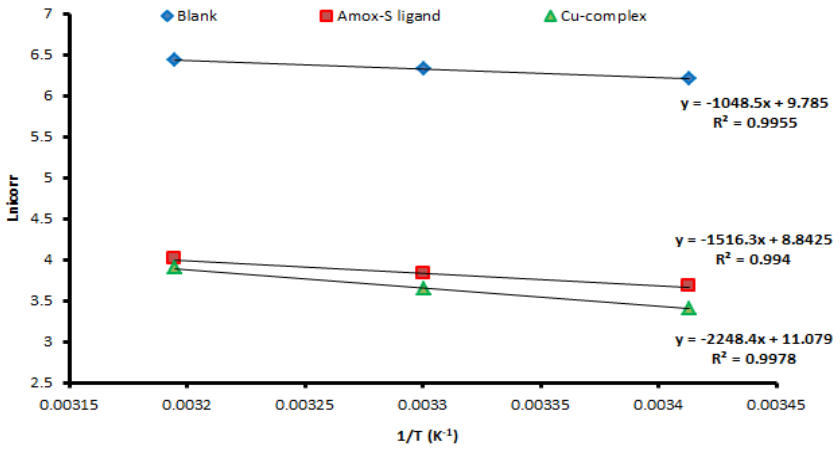

Figure 14. A plot of Lni_{corr} vs. 1/T for a blank, Amox-S ligand and its Cu(II)-complex at different temperatures

Thermodynamic parameters were analyzed via the transition state (equation 9) (Raheema et al., 2023), which provided the enthalpy (ΔH*) and entropy (ΔS*) of activation.

$$\ln\left(\frac{icorr}{T}\right) = \ln\left(\frac{R}{Nh}\right) + \frac{\Delta S*}{R} - \frac{\Delta H*}{R}\left(\frac{1}{T}\right) \tag{9}$$

From equation 10, the Gibbs free energy (ΔG*) was estimated.

$$\Delta G^* = \Delta H^* - T\,\Delta S^* \quad (10)$$

Where (icorr) is the corrosion current density, (ΔS*) is the entropy, (ΔH*) is the enthalpy, h is Planck's constant, N is the Avogadro number, R is the universal gas constant and T is the absolute temperature (K). A plot of ln(icorr/T) vs 1/T of equation 9 provides straight lines for calculating values of ΔH* and ΔS* for blank and inhibitors, as shown in Figure 15. The positive ΔH* values for all systems (6.2 kJ/mol for blank, 10.09 kJ/mol for Amox-S, and 16.8 kJ/mol for Cu(II)-complex showed that the corrosion process absorbs heat and needs energy, and this need is greater when inhibitors are present. These results correlate with the increased energy barrier needed for corrosion in inhibited systems (Adamu et al., 2025).

The entropy of activation (ΔS*) showed negative values across all samples, with −172 J/mol.K for the blank, and much more negative values for Amox-S (−179.84J/mol•K) and CuL1 (−161.24 J/mol.K). The negative ΔS* values indicate a decrease in system disorder during the transition from reactants to the activated complex, characteristic of adsorption-controlled processes. The more negative ΔS* observed in the presence of inhibitors suggests increased molecular ordering associated with the formation of a stable and compact protective film on the metal surface (Olasunkanmi et al., 2020). The negative ΔG* values across all temperatures confirm the spontaneous nature of the corrosion process. However, these values become less negative in the presence of inhibitors—shifting at 293 K from −8.24 kJ/mol (blank) to −2.06 kJ/mol for Amox-S and −1.42 kJ/mol for the Cu(II) complex—indicating thermodynamic suppression of corrosion (Praveen et al., 2025). The kinetic and thermodynamic parameters (Table 9) further confirm that both inhibitors act via adsorption mechanisms. The Cu(II) complex exhibits predominantly chemisorptive behavior due to stronger metal–inhibitor interactions, whereas the ligand shows mixed physisorption–chemisorption characteristics. These results highlight the superior inhibition efficiency of the complex and emphasize the influence of molecular structure on thermal stability and corrosion protection performance.

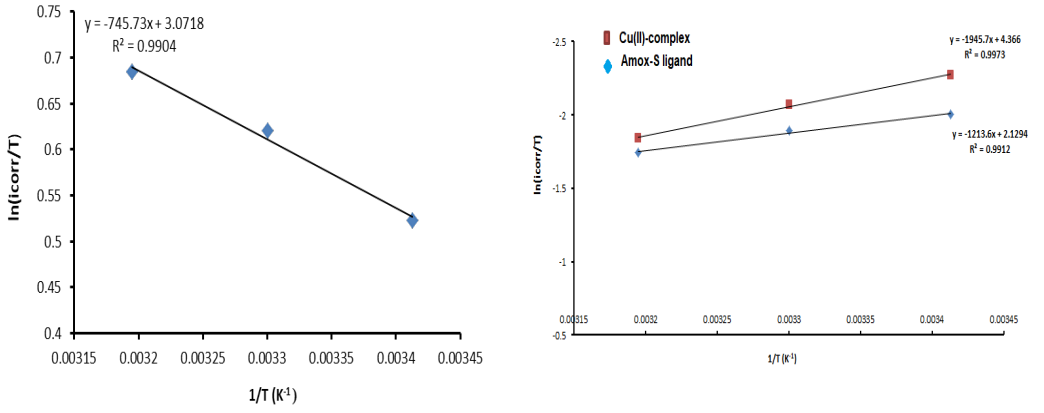

Figure 15. A plot of Lnicorr/T vs. 1/T for a blank, Amox-S ligand and its Cu(II)-complex at different temperatures

Table 9. Kinetic and thermodynamic analysis of the corrosion ınhibition process

Sample	T(K)	Ea(kJ/mole)	ΔH*(kJ/mole)	ΔS*(J/mole.K)	ΔG*(kJ/mole)
Blank	**293**	8.717	6.2	-172	-8.24499
	303				-8.7379
	313				-9.22744
Amox-S	**293**	12.6	10.09	-179.84	-2.0561
	303				-2.47064
	313				-2.88518
Cu-complex	**293**	18.69	16.18	-161.24	-1.41778
	303				-2.01827
	313				-2.61876

3.8 Surface examination

SEM analysis was performed using a scanning electron microscope equipped with a high-vacuum system and a tungsten/field emission electron gun, providing high-resolution images of the sample surface. The surface morphology of the metal samples immersed in acidic solution for 10 days, with and without the corrosion inhibitor. The surface morphology of the prepared samples was examined to evaluate the protective performance of the inhibitor. Figure 16(a) shows the SEM image of the C45 steel specimen after 10 days immersion in 1 M HCl solution. The observed surface roughness and corrosion visible lines indicated significant damage in the surface and absence of protective layer. This indicates that the surface was fully exposed to the acidic solution without any protection. Figure 16(b) and Figure 16(c) show the SEM of C45 specimen in $1x10^{-3}$ M of Amox-S ligand and Cu-complex inhibitors after 10 days of immersion. The surfaces appear smoother and less damaged compared to the unprotected samples. These solutions significantly improved the corrosion resistance of C45 steel that corroborates the high IE% of the inhibitors. These findings show that the presence of inhibitors molecules get adsorbed onto the surface and form a layer of protection (Ladan et al., 2025).

4. Conclusions

Metal complexes, particularly Au(III) and Cu(II), functioned better as antioxidants at lower concentrations than ascorbic acid, showing that they may be used in therapies that require small amounts to be effective. Amox-S and its Cu-complex approached similar levels of activity at higher concentrations, which made them intriguing possibilities for use as artificial antioxidants. The results also indicate the importance of complex stability and redox behavior in determining long-term antioxidant efficiency, leading to the need for more structural and mechanistic research.

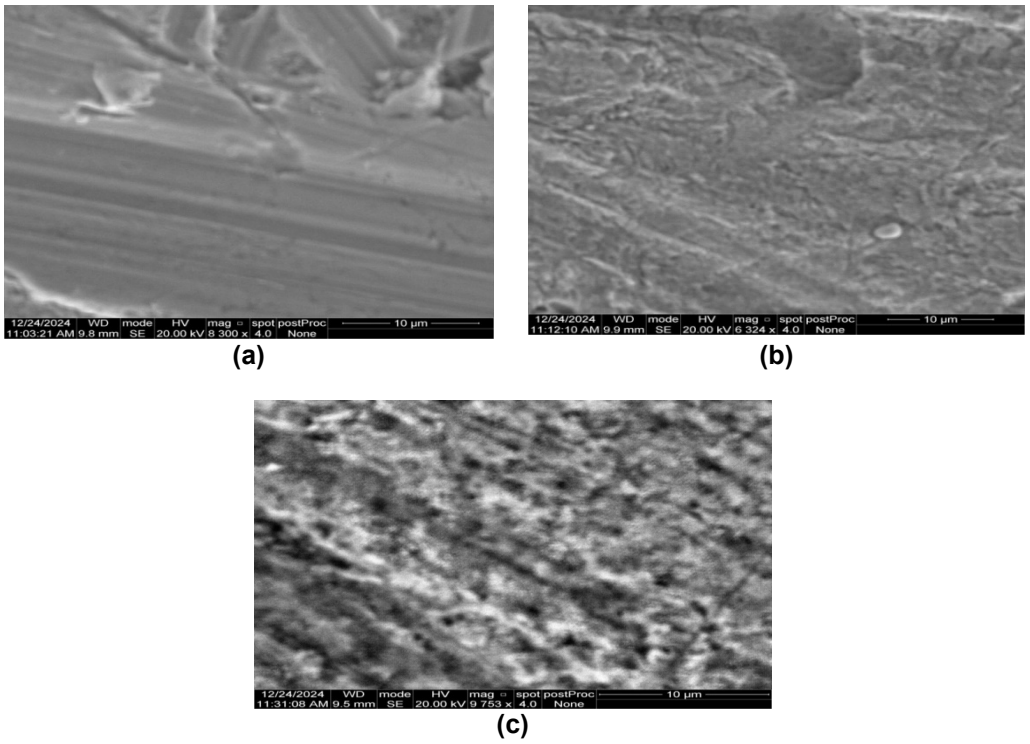

Figure 16. The SEM of (a) Carbon mild steel (C45) in 1M HCl without inhibitors, (b) in the presence of $1x10^{-3}$ M of Amox-S ligand, and (c) in the presence of $1x10^{-3}$ M of Cu-complex

The Schiff base ligand derived from amoxicillin and its copper complex significantly reduced the corrosion rate of C45 mild steel in acidic solution. The Cu-complex consistently outperformed Amox-S likely due to better adsorption and film-forming capabilities. Thermodynamic and kinetic evaluations supported the formation of a protective film on the steel surface, which inhibited both anodic and cathodic corrosion processes. These findings suggest that Amox-S and especially its Cu-complex are effective and thermally stable corrosion inhibitors for mild steel in acidic environments. The polarization and weight loss study supported the effectiveness of inhibition in the following sequence Cu-complex> Amox-S > Blank. Inhibition is mixed type, with stronger cathodic suppression and efficiency is thermally stable, implying chemisorption rather than mere physisorption.

5. Authors' Contributions

Hawraa M. Alabidi designed research, performed research, coordinated research; and wrote the paper; Layla Ali Mohammed contributed new reagents/analytic tools, analyzed data.

ORCID

Hawraa M. Alabidi https://orcid.org/0000-0002-6805-8482

6. Conflicts of Interest

The authors declare no conflicts of interest.

References

Abd El-Zahir, M. S., Soliman, M. H. A., ELKady, H. A., El-Sakka, S. S. A., & Orabi, A. S. (2024). New inorganic inhibitors derived from cefotaxime to enhance corrosion resistance of mild steel in 3% NaCl. *Scientific Reports*, *14*(1), Article 950. https://doi.org/10.1038/s41598-024-51275-5

Abdallah, M., Soliman, K. A., Alfakeer, M., Hawsawi, H., Al-Bonayan, A. M., Al-Juaid, S. S., El Wanees, S. A., & Motawea, M. S. (2023). Expired antifungal drugs as effective corrosion inhibitors for carbon steel in 1 M HCl solution: practical and theoretical approaches. *ACS Omega*, *8*(38), 34516-34533. https://doi.org/10.1021/acsomega.3c03257

Adamu, A. A., Iyun, O. R. A., & Habila, J. D. (2025). Adsorption and thermodynamic studies of the corrosion Inhibition effect of *Desmodium adscendens* (Swartz) extract on carbon steel in 2 M HCl. *BMC Chemistry*, *19*(1), Article 163. https://doi.org/10.1186/s13065-025-01541-y

Affat, S. S. (2022). Experimental and theoretical studies of new Schiff base as a corrosion inhibitor in acidic media and study antioxidant activity. *Iranian Journal of Chemistry and Chemical Engineering*, *41*(10), 3351-3364. https://doi.org/10.30492/ijcce.2021.534910.4860

Ahmed, M. A., Amin, S., & Mohamed, A. A. (2024). Current and emerging trends of inorganic, organic and eco-friendly corrosion inhibitors. *RSC Advances*, *14*(43), 31877-31920. https://doi.org/10.1039/d4ra05662k

Alabidi, H. M., Alabidi, A. M., & Makki, N. (2018). Synthesis and spectroscopic studying of new azo ligand from 2-naphthol derivative and it's complexes with some transition metal ions. *Al-Qadisiyah Journal of Pure Science*, *23*(1), 186-195. https://doi.org/10.29350/jops.2018.23.1.731

Alabidi, H. M., Farhan, A. M., Al-labban, H. M. Y., & Aljanaby, A. A. J. (2023). New derivatives from 4-amino anti-pyrine and vanillin, synthesis characterization and antibacterial activity. *Egyptian Journal of Chemistry*, *66*(1), 175-181. https://doi.org/10.21608/EJCHEM.2022.135727.5977

Al-Amiery, A. A., Al-Azzawi, W. K., & Isahak, W. N. R. W. (2022). Isatin Schiff base is an effective corrosion inhibitor for mild steel in hydrochloric acid solution: gravimetrical, electrochemical, and computational investigation. *Scientific Reports*, *12*(1), Article 17773. https://doi.org/10.1038/s41598-022-22611-4

Alamry, K. A., Khan, A., Aslam, J., Hussein, M. A., & Aslam, R. (2023). Corrosion inhibition of mild steel in hydrochloric acid solution by the expired ampicillin drug. *Scientific Reports*, *13*(1), Article 6724. https://doi.org/10.1038/s41598-023-33519-y

Al-Daffay, R. K. H., Al-Hamdani, A. A. S., & Elluhaibi, E. A. E. (2025). Synthesis, characterization and studying thermal analysis for complexes of some metal ions and determining their activity as antioxidants. *Baghdad Science Journal*, *22*(3), 801-812. https://doi.org/10.21123/bsj.2024.9644

Alfakeer, M., Abdallah, M., & Fawzy, A. (2020). Corrosion inhibition effect of expired ampicillin and flucloxacillin drugs for mild steel in aqueous acidic medium. *International Journal of Electrochemical Science*, *15*(4), 3283-3297. https://doi.org/10.20964/2020.04.09

Ali, M., Sholkamy, E. N., Alobaidi, A. S., Al-Muhanna, M. K., & Barakat, A. (2023). Synthesis of Schiff bases based on chitosan and heterocyclic moiety: Evaluation of antimicrobial activity. *ACS Omega*, *8*(49), 47304-47312. https://doi.org/10.1021/acsomega.3c08446

Almomani, M. A., Al-Noaimi, M., Hayajneh, M. T., Alshurafat, H. H., & Alshamaileh, E. M. (2021). Experimental evaluation of new organic compounds as corrosion inhibitors for mild steel in hydrochloric acid. *International Journal of Corrosion and Scale Inhibition*, *10*(3), 1141-1156. https://doi.org/10.17675/2305-6894-2021-10-3-18

Betti, N., Al-Amiery, A. A., Al-Azzawi, W. K., & Isahak, W. N. R. W. (2023). Corrosion inhibition properties of schiff base derivative against mild steel in HCl environment complemented with DFT investigations. *Scientific Reports*, *13*(1), Article 8979. https://doi.org/10.1038/s41598-023-36064-w

Chaudhary, N. K., & Mishra, P. (2017). Metal complexes of a novel Schiff base based on penicillin: characterization, molecular modeling, and antibacterial activity study. *Bioinorganic Chemistry and Applications*, *2017*(1), Article 6927675. https://doi.org/10.1155/2017/6927675

Chavelas-Hernández, L., Valdéz-Camacho, J. R., Hernández-Vázquez, L. G., Dominguez-Mendoza, B. E., Vasquez-Ríos, M. G., & Escalante, J. (2020). A new approach using aromatic-solvent-induced shifts in NMR spectroscopy to analyze β-lactams with various substitution patterns. *Synlett*, *31*(2), 158-164. https://doi.org/10.1055/s-0039-1691498

Diki, N. G. Y. S., Coulibaly, N. H., Kambiré, O., & Trokourey, A. (2021). Experimental and theoretical investigations on copper corrosion inhibition by cefixime drug in 1M HNO_3 solution. *Journal of Materials Science and Chemical Engineering*, *9*(5), 11-28. https://doi.org/10.4236/msce.2021.95002

El Aloua, A., Oubahou, M., El Bouari, A., & Tanane, O. (2024). Expired amoxicillin as an eco-friendly corrosion inhibitor for cast steel in sulfuric acid environment: electrochemical, surface and thermodynamic studies. *Journal of Solid State Electrochemistry*, *28*(7), 2397-2411. https://doi.org/10.1007/s10008-023-05788-0

El-Lateef, H. M. A., El-Dabea, T., Khalaf, M. M., & Abu-Dief, A. M. (2022). Innovation of imine metal chelates as corrosion inhibitors at different media: A collective study. *International Journal of Molecular Sciences*, *23*(16), Article 9360. https://doi.org/10.3390/ijms23169360

El-Lateef, H. M. A., El-Dabea, T., Khalaf, M. M., & Abu-Dief, A. M. (2023). Recent overview of potent antioxidant activity of coordination compounds. *Antioxidants*, *12*(2), Article 213. https://doi.org/10.3390/antiox12020213

Emrayed, H. F., Amraga, E. A., Ibrahim, D. M., & Fouda, A. E. A. S. (2025). Corrosion inhibition effect of Schiff base and its metal complexes with [Mn (II) and Cu (II)] on carbon steel in hydrochloric acid solution: Experimental and surface studies. *International Journal of Electrochemical Science*, *20*(1), Article 100912. https://doi.org/10.1016/j.ijoes.2024.100912

Farhan, A. M., Egzar, H. K., & Alabidi, H. M. (2024). New compounds derived from nitrophenol synthesis, structural investigation and anticorrision properties. *Acta Chimica Slovenica*, *71*(2), 179-185. https://doi.org/10.17344/acsi.2023.8489

Go, L. C., Depan, D., Holmes, W. E., Gallo, A., Knierim, K., Bertrand, T., & Hernandez, R. (2020). Kinetic and thermodynamic analyses of the corrosion inhibition of synthetic extracellular polymeric substances. *PeerJ Materials Science*, *2*, Article e4. https://doi.org/10.7717/peerj-matsci.4

Hadi, M. A., Mohammed, M. S., & Kadhium, A. J. (2021). Synthesis, characterization and spectral studies and biological screening study of transition metal complexes with new heterocyclic ligand derived from pyridoxal hydrochloride. *Systematic Reviews in Pharmacy*, *12*(1), 371-383.

Hernández, J. G., Aguilar, C. A. H., Narayanan, J., Flores, E. D. T., Thangarasu, P., Ramírez, A. H., Shammugam, K., & Martinez, M. M. L. (2024). Effect of metal ions in the electron-transfer mechanism on the photovoltaic performance of SALPHEN-

based DSSC: experimental and theoretical studies. *Materials Advances*, *5*(8), 3257-3280. https://doi.org/10.1039/d3ma00982c

Hilal, T. A. A., & Kareem, I. K. (2025). Synthesis of some metal complexes with new heterocyclic ligand (5-(((2-(3-(1 H-indol-3-yl) acryloyl) phenyl) amino) methylene)-2-thiooxodihydropyrimidine-4, 6 (1 H, 5 H)-dione) and their biological effectiveness as antioxidant and anti-cancer. *Indonesian Journal of Chemistry*, 25(1), 60-75. https://doi.org/10.22146/ijc.95731

Kalluru, S., Dammu, L. K., Nara, S. K., & Nimmagadda, V. V. J. (2023). Synthesis and characterization of Schiff base, 3-hydroxy-4-(3-hydroxy benzylidene amino) benzoic acid and their Ni (II) and Zn (II) metal complexes. *Journal of Advanced Scientific Research*, *14*(1), 35-39. https://doi.org/10.55218/JASR.202314105

Kanagavalli, C., Kalanithi, M., Gurusamy, S., Asha, R. N., Megtalin, N. M., & Sankarganesh, M. (2024). Computational, spectroscopic, sensor and biological studies of Cu (II) complex of Fluoro substituted Schiff base. *Chemical Physics Impact*, *8*, Article 100582. https://doi.org/10.1016/j.chphi.2024.100582

Karaman, R., Al-Kurd, S., Yaghmour, R., Amro, A., & Karaman, D. (2015). Antibacterial activity of novel prodrugs of amoxicillin and cephalexin. *World Journal of Pharmaceutical Research*, *4*(9), 334-360.

Kasare, M. S., Dhavan, P. P., Jadhav, B. L., & Pawar, S. D. (2019). Synthesis of azo Schiff base ligands and their Ni (II), Cu (II) and Zn (II) metal complexes as highly-active antibacterial agents. *ChemistrySelect*, *4*(36), 10792-10797. https://doi.org/10.1002/slct.201901605

Khudhair, N. A., & Al-Sammarraie, A. M. A. (2019). Enhancing of corrosion protection of steel rebar in concrete using TiO2 nanoparticles as additive. *Iraqi Journal of Science*, *60*(9), 1898-1903. https://doi.org/10.24996/ijs.2019.60.9.2

Khudhair, N. A., Bader, A. T., Ali, M. I., & Husseini, M. (2020). Synthesis, identification and experimental studies for carbon steel corrosion in hydrochloric acid solution for polyimide derivatives. *AIP Conference Proceedings*, *2290*(1), Article 030014. https://doi.org/10.1063/5.0027443

Kyhoiesh, H. A. K., & Al-Adilee, K. J. (2021). Synthesis, spectral characterization, antimicrobial evaluation studies and cytotoxic activity of some transition metal complexes with tridentate (N, N, O) donor azo dye ligand. *Results in Chemistry*, *3*, Article 100245. https://doi.org/10.1016/j.rechem.2021.100245

Kyhoiesh, H. A. K., & Al-Adilee, K. J. (2023). Pt (IV) and Au (III) complexes with tridentate-benzothiazole based ligand: synthesis, characterization, biological applications (antibacterial, antifungal, antioxidant, anticancer and molecular docking) and DFT calculation. *Inorganica Chimica Acta*, *555*, Article 121598. https://doi.org/10.1016/j.ica.2023.121598

Kzar, W. D., Mohammed, H. S., Zghair, F. S., & Zizi, Z. (2023). Synthesis, characterization and staining ability of novel azo dye based on curcumin and its Au (III) complex. *Indonesian Journal of Chemistry*, *23*(5), 1375-1383. https://doi.org/10.22146/ijc.84388

Ladan, M., Ayuba, A. M., & Zakariyya, D. (2025). Evaluation of corrosion inhibition potential of Schiff bases derived from 2-hydroxybenzaldehyde on mild steel in 1M HCl solution. *Journal of Materials and Environmental Science*, *16*(2), 304-319.

Lasri, M., Hassnaoui, A., Idlahoussaine, N., Ait-Karra, A., Maatallah, M., Zakir, O., Idouhli, R., Khadiri, M. E., Ali, M. A., & Abouelfida, A. (2025). Novel Schiff base derivatives: Enhanced corrosion protection for copper in NaCl solutions–electrochemical insights and theoretical analysis. *Journal of Industrial and Engineering Chemistry*, *146*, 551-563. https://doi.org/10.1016/j.jiec.2024.11.039

Mahmoud, Z. S., Shams, A. K., & Salman, T. A. (2022). Study the inhibition effect of amoxicillin drug for corrosion of carbon steel in saline media. *Baghdad Science Journal*, *19*(1), Article 9. https://doi.org/10.21123/bsj.2022.19.1.0121

Malik, M. A., Dar, O. A., Gull, P., Wani, M. Y., & Hashmi, A. A. (2018). Heterocyclic Schiff base transition metal complexes in antimicrobial and anticancer chemotherapy. *MedChemComm*, *9*(3), 409-436. https://doi.org/10.1039/C7MD00526A

Moreno-Narváez, M. E., González-Sebastián, L., Colorado-Peralta, R., Reyes-Márquez, V., Franco-Sandoval, L. O., Romo-Pérez, A., Cruz-Navarro, J. A., Mañozca-Dosman, I. V., Aragón-Muriel, A., & Morales-Morales, D. (2025). Anticancer and antimicrobial activity of copper(ii) complexes with fluorine-functionalized Schiff bases: A mini-review. *Inorganics*, *13*(2), Article 38. https://doi.org/10.3390/inorganics13020038

Mushtaq, I., Ahmad, M., Saleem, M., & Ahmed, A. (2024). Pharmaceutical significance of Schiff bases: an overview. *Future Journal of Pharmaceutical Sciences*, *10*, Article 16. https://doi.org/10.1186/s43094-024-00594-5

Olasunkanmi, L. O., Idris, A. O., Adewole, A. H., Wahab, O. O., & Ebenso, E. E. (2020). Adsorption and corrosion inhibition potentials of salicylaldehyde-based Schiff bases of semicarbazide and p-toluidine on mild steel in acidic medium: Experimental and computational studies. *Surfaces and Interfaces*, *21*, Article 100782. https://doi.org/10.1016/j.surfin.2020.100782

Patriarca, C., & Hawkes, J. A. (2020). High molecular weight spectral interferences in mass spectra of dissolved organic matter. *Journal of the American Society for Mass Spectrometry*, *32*(1), 394-397. https://doi.org/10.1021/jasms.0c00353

Podolski-Renić, A., Gašparović, A. Č., Valente, A., López, Ó., Nunes, J. H. B., Kowol, C. R., Heffeter, P., & Filipović, N. R. (2024). Schiff bases and their metal complexes to target and overcome (multidrug) resistance in cancer. *European Journal of Medicinal Chemistry*, *270*, Article 116363. https://doi.org/10.1016/j.ejmech.2024.116363

Praveen, B. M., Jeevan Chakravarthy, A. S., Prasanna, B. M., Shabanbanu, Devendra, B. K., Pavithra, M. K., & Fasiulla. (2025). Experimental and theoretical investigation of cyclohexanone derivative (CHD) as a corrosion inhibitor for mild steel in 1 M HCl. *Scientific Reports*, *15*(1), Article 720. https://doi.org/10.1038/s41598-024-83054-7

Presenjit, Chaturvedi, S., Singh, A., Gautam, D., Singh, K., & Mishra, A. K. (2024). An insight into the effect of Schiff Base and their d and f block metal complexes on various cancer cell lines as anticancer agents: A review. *Anti-cancer Agents in Medicinal Chemistry*, *24*(7), 488-503. https://doi.org/10.2174/0118715206280314231201111358

Radi, A., El Mahi, B., Aouniti, A., El Massoudi, M., Radi, S., Kaddouri, M., Chelfi, T., Jmiai, A., El Asri, A., Hammouti, B., Warad, I., Guenbour, A., & Zarrouk, A. (2022). Mitigation effect of novel bipyrazole ligand and its copper complex on the corrosion behavior of steel in HCl: Combined experimental and computational studies. *Chemical Physics Letters*, *795*, Article 139532. https://doi.org/10.1016/j.cplett.2022.139532

Raheema, M. H., Khudhair, N. A., AL-Noor, T. H., Al-Ayash, S. R., Kharnoob, H. H., & Obed, S. M. (2023). Enhancement of corrosion protection of metal carbon steel C45 and stainless steel 316 by using inhibitor (Schiff base) in sea water. *Baghdad Science Journal*, *20*(3), Article 30. https://doi.org/10.21123/bsj.2023.7749

Ramadan, R. M., El-Shalakany, H. H. & Sayed, M. A. (2025). Structural and biomedical investigations of novel ruthenium schiff base complexes. *Scientific Reports*, *15*, Article 18546. https://doi.org/10.1038/s41598-025-03147-9

Reiss, A., Chifiriuc, M. C., Amzoiu, E., & Spînu, C. I. (2014). Transition metal (ii) complexes with cefotaxime-derived Schiff Base: Synthesis, characterization, and antimicrobial studies. *Bioinorganic Chemistry and Applications*, *2014*(1), Article 926287. https://doi.org/10.1155/2014/926287

Reiss, A., Samide, A., Ciobanu, G., & Dabuleanu, I. (2015). Synthesis, spectral characterization and thermal behaviour of new metal (II) complexes with Schiff base derived from amoxicillin. *Journal of the Chilean Chemical Society*, *60*(3), 3074-3079.

Savcı, A., Buldurun, K., Alkış, M. E., Alan, Y., & Turan, N. (2022). Synthesis, characterization, antioxidant and anticancer activities of a new Schiff base and its M(II) complexes derived from 5-fluorouracil. *Medical oncology*, *39*(11), Article 172. https://doi.org/10.1007/s12032-022-01774-0.

Shwetha, K. M., Praveen, B. M., & Devendra, B. K. (2024). A review on corrosion inhibitors: types, mechanisms, electrochemical analysis, corrosion rate and efficiency of corrosion inhibitors on mild steel in an acidic environment. *Results in Surfaces and Interfaces*, *16*, Article 100258. https://doi.org/10.1016/j.rsurfi.2024.100258

Soroceanu, A., & Bargan, A. (2022). Advanced and biomedical applications of Schiff-Base ligands and their metal complexes: A review. *Crystals*, *12*(10), Article 1436. https://doi.org/10.3390/cryst12101436

Tabrizi, L., Dao, D. Q., & Vu, T. A. (2019). Experimental and theoretical evaluation on the antioxidant activity of a copper (II) complex based on lidocaine and ibuprofen amide-phenanthroline agents. *RSC Advances*, *9*(6), 3320-3335. https://doi.org/10.1039/c8ra09763a

Todorov, L., Saso, L., & Kostova, I. (2023). Antioxidant activity of coumarins and their metal complexes. *Pharmaceuticals*, *16*(5), Article 651. https://doi.org/10.3390/ph16050651

Verma, C., Al-Moubaraki, A. H., Alfantazi, A., & Rhee, K. Y. (2024). Heterocyclic amino acids-based green and sustainable corrosion inhibitors: Adsorption, bonding and corrosion control. *Journal of Cleaner Production*, *446*, Article 141186. https://doi.org/10.1016/j.jclepro.2024.141186

Younus, H. A., Saleem, F., Hameed, A., Al-Rashida, M., Al-Qawasmeh, R. A., El-Naggar, M., Khan, K. M. (2023). Part-II: an update of Schiff bases synthesis and applications in medicinal chemistry-a patent review (2016-2023). *Expert Opinion on Therapeutic Patents*, *33*(12), 841-864. https://doi.org/10.1080/13543776.2023.2297729

Youssif, M. M., El-Nahass, M. N., Fayed, T. A., El-Daly, H. A., El-Gamil, M. M., & Eldesoky, A. M. (2023). Tunable anticorrosive effects of newly synthesized Benzothiazole Azo dyes by potassium iodide synergism for carbon steel in 1 M HCl: Combined experimental and theoretical studies. *ACS Omega*, *8*(31), 28314-28332. https://doi.org/10.1021/acsomega.3c02105